Combustion and Flame 158 (2011) 354–368

Contents lists available at ScienceDirect

Combustion and Flame

journal homepage: www.elsevier.com/locate/combustflame

Combustion characteristics of fuel droplets with addition of nano and micron-sized aluminum particles

Yanan Gan, Li Qiao *

School of Aeronautics & Astronautics, Purdue University, West Lafayette, IN 47907, United States

ARTICLE INFO

Article history:
Received 13 June 2010
Received in revised form 27 July 2010
Accepted 3 September 2010

Keywords:
High-energy-density fuels
Droplet combustion
Aluminum nanoparticles
Microexplosion
Particle aggregation

ABSTRACT

The burning characteristics of fuel droplets containing nano and micron-sized aluminum particles were investigated. Particle size, surfactant concentration, and the type of base fluid were varied. In general, nanosuspensions can last much longer than micron suspensions, and ethanol-based fuels were found to achieve much better suspension than *n*-decane-based fuels. Five distinctive stages (preheating and ignition, classical combustion, microexplosion, surfactant flame, and aluminum droplet flame) were identified for an *n*-decane/nano-Al droplet, while only the first three stages occurred for an *n*-decane/micron-Al droplet. For the same solid loading rate and surfactant concentration, the disruption and microexplosion behavior of the micron suspension occurred later with much stronger intensity. The intense droplet fragmentation was accompanied by shell rupture, which caused a massive explosion of particles, and most of them were burned during this event. On the contrary, for the nanosuspension, combustion of the large agglomerate at the later stage requires a longer time and is less complete because of formation of an oxide shell on the surface. This difference is mainly due to the different structure and characteristics of particle agglomerates formed during the early stage, which is a spherical, porous, and more-uniformly distributed aggregate for the nanosuspension, but it is a densely packed and impermeable shell for the micron suspension. A theoretical analysis was then conducted to understand the effect of particle size on particle collision mechanism and aggregation rate. The results show that for nanosuspensions, particle collision and aggregation are dominated by the random Brownian motion. For micron suspensions, however, they are dominated by fluid motion such as droplet surface regression, droplet expansion resulting from bubble formation, and internal circulation. And the Brownian motion is the least important. This theoretical analysis explains the different characteristics of the particle agglomerates, which are responsible for the different microexplosion behaviors that were observed in the experiments.

© 2010 The Combustion Institute. Published by Elsevier Inc. All rights reserved.

1. Introduction

Metals such as aluminum have higher combustion energies and have been employed as energetic additives in propellants and explosives [1]. Recent advances in nanoscience and nanotechnology enable production, control, and characterization of nanoscale energetic materials, which have shown tremendous advantages over micron-sized materials. Because of the high specific surface area, metal nanoparticles offer shortened ignition delays, decreased burn times, and more complete combustion than micron-sized particles [1–3].

Using nanoscale energetic materials as fuel additives to enhance combustion of traditional liquid fuels is an interesting concept. The high energy density of metals, particularly aluminum, could significantly improve power output of engines and thus reduce consumption of liquid fuels and consequently result in less CO_2, NO_x, etc. In addition to higher energy density, fuel additives have potentials to shorten ignition delay time and enhance fuel oxidation by catalytic effect. Studies on ignition and combustion behavior of liquid fuels with nanoscale additives, however, are rare. Tyagi et al. [4] used a simple hot-plate experiment to study the effects on the ignition properties of diesel fuel when small quantities of aluminum and aluminum oxide nanoparticles were added. It was observed that the ignition probability for the fuel mixtures containing nanoparticles was significantly higher than that of pure diesel. Beloni et al. [5] recently studied combustion of decane-based slurries with metallic nano additives using a lifted laminar flame burner, considering pure aluminum, mechanically alloyed $Al_{0.7}Li_{0.3}$, and nanocomposite 2B + Ti as additives. Their effects on flame length, flame speed, flame emissions, and temperatures were measured. These studies, though limited, have shown promise of

* Corresponding author. Address: Neil Armstrong Hall of Engineering, School of Aeronautics & Astronautics, 701 W. Stadium Ave., Purdue University, West Lafayette, IN 47907, United States. Fax: +1 765 494 0307.
E-mail address: lqiao@purdue.edu (L. Qiao).

0010-2180/$ - see front matter © 2010 The Combustion Institute. Published by Elsevier Inc. All rights reserved.
doi:10.1016/j.combustflame.2010.09.005

using nanoscale additives to enhance the combustion of liquid fuels.

Slurry fuels, which are mixtures of liquid and solid fuels, were under serious consideration as high-energy fuels a few decades ago. Aluminum, boron, and carbon particles (5–200 μm) were added to liquid fuels as a "liquid fuel extender" in the sense that less hydrocarbon and more plentiful solid fuel (e.g., coal) can be used [6]. The burning characteristics of slurry droplets involving micron-sized boron [7–10], aluminum [11–13], carbon, and a blend of aluminum and carbon [14–17] particles at relatively high solid loadings (40–80 wt.%) were studied experimentally. A few theories and postulates were proposed based on the experimental observations [10,18,19], and a review was provided by Choudhury [6]. In general, during the initial phase of oxidation of the droplet, semiporous hollow shells or densely packaged shells, consisting of the particle agglomerates, may form and thereby cause an increase in diameter as a result of swelling. Solid particles, heated by flame radiation and/or exothermic reaction, may initiate local boiling or liquid phase decomposition at the surface. Several possible events can take place, either individually or jointly, during slurry droplet combustion. A key event is the disruption/microexplosion behavior, which was first discovered by Takahashi et al. [8] for slurries of boron/JP-10 droplets. Two boron samples, amorphous (0.20–0.32 μm) and crystalline (3.57 μm), were used in the experiment. This study demonstrated that disruption of the primary droplet results in secondary atomization, which substantially enhances the overall burning rate of the primary droplet and provides a means for dispersal and ignition of the boron. This behavior was also evidenced by a few other studies involving aluminum and carbon slurries [13,17].

These previous studies have revealed some general burning characteristics of slurry fuels involving micron-sized particles. However, many puzzles remain. The events that can take place either individually or jointly during slurry droplet combustion have not been understood clearly [6] because of the complexity of the three-phase physics. Furthermore, other issues have not yet been fully studied, e.g., slurry preparation, slurry rheology, effects of surfactants on suspension quality and on combustion behavior, reaction kinetics and mechanisms of metal particles/agglomerates, and particle agglomeration mechanisms within a combusting droplet. Significantly, no studies have been made of slurry droplets involving nanoparticles, which could be different because of energy conversion and particle dynamics at different length scales, nano vs. micron.

The idea of the present paper is to suspend metallic nanoparticles in liquid fuels and to explore the differences between nanosuspensions and micron suspensions that have been studied previously. Nanoparticles have shown such advantages as higher reactivity and burning rate over micron-sized particles. But more important, nanoparticles are much easier to disperse and suspend in liquid fuels than microparticles are, the latter tending to settle quickly as a result of gravity. This is because nanoparticles have an extremely high ratio of surface area to volume; thus the interaction between particle surface and the surrounding liquid is strong enough to overcome difference in density. Moreover, the larger surface area of nanoparticles can be utilized for surface functionalization, making stabilized suspension possible to maintain for a very long time in practical applications. Also, ionic groups in liquid fuel can be absorbed onto particle surfaces to form a charged layer, which results in repulsive forces. These forces between nanoparticles increase as a result of the larger specific surface areas of nanoparticles, and this may reduce agglomeration to some extent [20]. The dispersion and suspension of metal nanoparticles in liquids have been critical issues in nanofluids research, which uses metal nanoparticles to enhance thermal conductivity of liquids for better cooling of micro- and nano-electromechanical systems (MEMS or NEMS), power electronics, light-emitting diodes, and semiconductor lasers [21].

The objectives of the present study are: (1) to investigate dispersion and suspension of nanoparticles in various liquid fuels and (2) to explore the difference between nanosuspension (<100 nm) and micron suspension (1–200 μm), especially the effect of particle size on droplet burning characteristics. The paper starts with fuel formulation methods, including particle dispersion, deagglomeration and fuel characterization. The droplet combustion experiment and diagnostic methods are then described. Several distinctive combustion stages are identified for the general burning behavior of a nanosuspension. The effects of surfactant and base fluid on suspension quality and droplet burning characteristics are discussed. In particular, the burning behavior of nanosuspensions was compared to that of micron suspensions. The results show that the characteristics and structures of particle agglomerates formed during droplet evaporation and combustion are responsible for the different burning behaviors. Lastly, a theoretical analysis is conducted to provide understanding of particle collision mechanisms and aggregate rates within a droplet. This analysis further reveals the effect of particle size on agglomeration formation and burning, which is consistent with the present experimental observations.

2. Experimental method

2.1. Fuel preparation and characterization

The preparation of fuel mixtures, a key step in developing knowledge of the nanofluid-type fuels, does not simply mean to disperse particles in liquids. Special handling is needed to achieve homogeneous, stable, long-term suspension and a low level of particle agglomeration. Many studies have shown that sonication and the adding of surfactants can reduce the coagulation of nanoparticles in nanofluids. The theory of ultrasonic-induced cavitation in liquids is well known [22]. When a liquid is exposed to ultrasound, the sound waves that propagate into it result in alternating high-pressure and low-pressure cycles. This applies mechanical stress to the attracting forces between the individual particles and thus separates the particles from one another and reduces agglomeration. Adding a surfactant to the mixture can promote chemical stabilization of the suspension. The mechanism is to overcome the van der Waals force between particles that leads to agglomeration by changing the surface properties of the suspended particles with a chemical agent [23]. The addition of surfactants can also significantly affect the combustion behavior of the fuel suspension, which will be discussed later.

Two liquid fuels, *n*-decane and ethanol, were considered as the base fluid. Aluminum particles of various sizes (mean diameters of 80 nm, 5 μm, and 25 μm) were considered as additives. The particles were naturally passivated with a thin layer of Al_2O_3 with a thickness of 2–8 nm and used as received with no further treatment. The active Al contents in the 80-nm and 5-μm Al samples were estimated to be 51.2–85.7% and 99.7–99.9% respectively. Figure 1a is a SEM photograph of the 80-nm Al sample (from Nanostructureed & Amorphous Materials, Inc.), which shows that the sample contains Al particles in the range of 35–100 nm, most of which are spherical and have a smooth surface. Figure 1b is a SEM photograph of the 5-μm Al sample (from Skylighter, Inc.), which shows that it has a wide size distribution in a range of 0.3–15 μm.

The particles were mixed with liquid fuels by first stirring them vigorously. Then an ultrasonic disruptor (Sharpertek, SYJ-450D) was used to disperse particles evenly and to avoid agglomeration. Sonication was performed in an ice bath to maintain a constant temperature for the mixture. The sonicator, which generates a series of 4-s-long pulses 4 s apart, was turned on for about 5 min. The

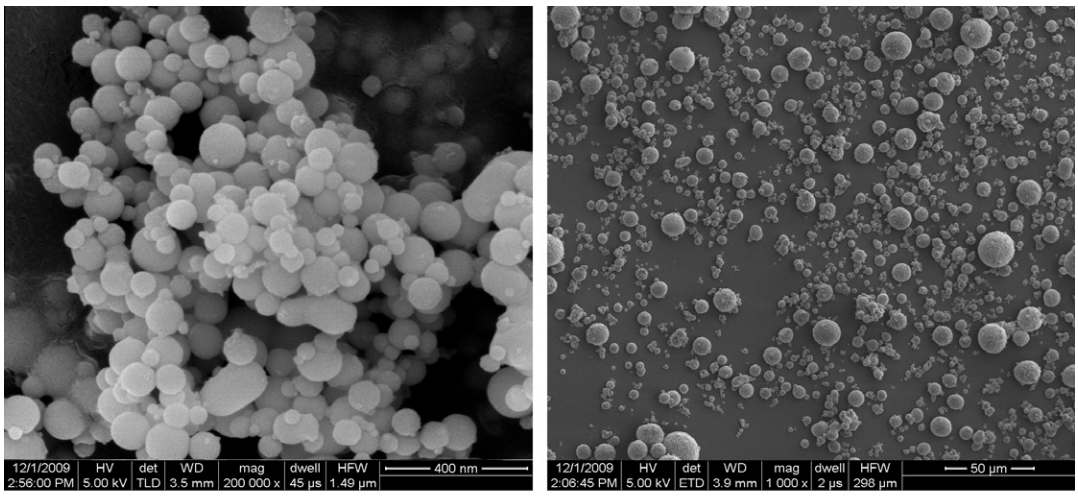

Fig. 1. SEM photographs of the two aluminum samples: (a) nanoparticles with a mean diameter of 80 nm; (b) micron-sized particles with a mean diameter of 5 μm.

dispersion characteristics of the suspension after sonication were evaluated during a period of observing potential sedimentation in a test tube. With sonication, suspensions of *n*-decane/nano-Al typically can remain stable for about 10 min, beyond which the particles will start to settle. After 60 min, all particles will have settled on the bottom of the test tube. Micron-Al particles, which will all settle on the bottom of the test tube in less than 5 min, are much easier to settle than nanoparticles. Suspensions of ethanol/nano-Al can last for 24 h without obvious sediment, much longer than *n*-decane/nano-Al. This could be because of ethanol's ability to easily wet nano-Al particles with its high extraction power [24], and this ability may lead to the formation of weak gel structures around the particles. As a result, the sedimentation of the particles will be retarded and a stable suspension can be achieved. Another reason is that ethanol has a higher viscosity than *n*-decane (1.2 vs. 0.92 mPa s at room temperature and atmospheric pressure). Particles in ethanol move slower because of higher viscous force; thus the sedimentation rate is lower.

To reduce particle agglomeration, we used Sorbitan Oleate ($C_{24}H_{44}O_6$) as a surfactant, which is a typical surfactant used to enhance the stability of metal nanoparticles in *n*-alkanes, and it is also commonly used in water/fuel emulsion [25]. It has a hydrophilic-lipophilic balance (HLB) value of 4.3 and is soluble with oil. Its physical properties, e.g., boiling point and viscosity, are compared with the base fluids *n*-decane and ethanol in Table 1. Sorbitan Oleate was mixed with the liquid fuel first, and then particles were added. After that, the suspension was sonicated by following the steps described above. The maximum concentration of the surfactant was 2.5 wt.%. With even 1 wt.% surfactant, the *n*-decane/nano-Al suspension can maintain homogeneity for at least 3 h, significantly longer than the suspension without surfactant, because of the steric stabilization mechanism [26]. Long-chain surfactant molecules attach to the particle surfaces, and an absorbed layer is formed around the particles. An overlap of the surfactant layer will produce the repulsive forces to overcome the universal van der Waals attraction; thus stability is maintained. It is noted that a sufficient amount of surfactant should be added to form a layer around each particle to produce the repulsive forces. However, too much surfactant will form macromolecules (a long-chain molecule group) that are free in the solution, which is called depletion stabilization [26]. Depletion stabilization is not desirable in this study, since we expect the major components of the mixture to be liquid fuel and aluminum particles.

Table 1
Physical properties of *n*-decane, ethanol and Sorbitan Oleate.

	Chemical formula	Molecular weight	Boiling point (K at 1 atm)	Viscosity (mPa s at 20 °C)
n-Decane	$C_{10}H_{22}$	142	447	0.92
Ethanol	C_2H_6O	46	352	1.2
Sorbitan Oleate	$C_{24}H_{44}O_6$	428	852	1200–2000

2.2. Experimental setup

Figure 2 shows a schematic diagram of the droplet combustion experiment. The experiments were performed in a closed cylindrical stainless-steel chamber of a volume of 0.0335 m^3. It has four quartz windows for optical access. The volume of the chamber is much larger than that of the droplets, thus the effect of droplet combustion on gas environment is neglected. A silicon carbide (Si–C) fiber with a diameter of 78 μm was used to suspend the droplet. Si–C fiber was chosen because of its low conductivity compared to metal wires. Ignition was achieved using a heating wire located directly beneath the droplet, which is made of nickel and chromium alloy with a resistance of about 1.5 Ω. A solenoid device was used to move the heating wire away immediately after the droplet was ignited.

The droplets were ignited in air at atmospheric pressure. The burning process was recorded by two orthogonally located high-speed digital cameras (a monochrome Phantom V7.3 camera with a speed of 6688 fps at a resolution of 800 × 600 and a color Photron Fastcam camera with a speed of 1000 fps at a resolution of 512 × 512). One camera was for direct imaging of the flame, and the other was with backlight for better determination of droplet size and observation of droplet disruption/breakup. The images were analyzed by Phantom Image software. To measure droplet temperature history, we used a type K thermocouple made of platinum (Pt) and platinum–rhodium (Pt–Rh) wires of 75 μm to suspend the droplet, instead of using both an Si–C fiber and a thermocouple to minimize the intrusion to the droplet. A 1000 Hz data acquisition system recorded the temperature history, which was synchronized with the high-speed digital camera to ensure that the droplet size and temperature history were measured simultaneously.

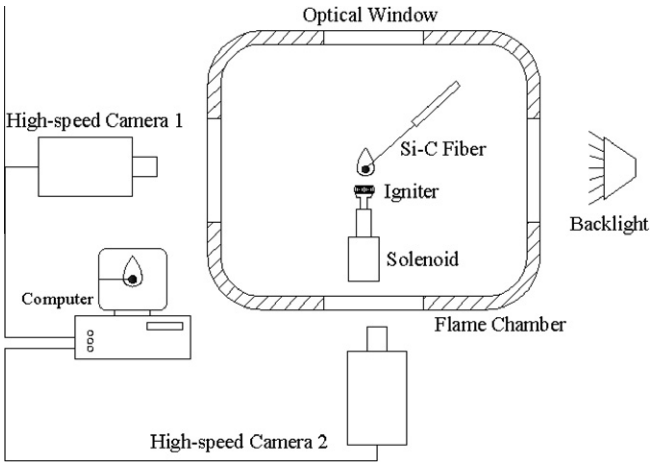

Fig. 2. Schematic of the experimental setup.

3. Results and discussion

3.1. Distinctive combustion stages for nanosuspension

Figure 3 shows the burning sequence of a stabilized *n*-decane/nano-Al droplet. The particle concentration is 10 wt.%, and the surfactant concentration is 2.5 wt.%. The droplet size and temperature histories are shown in Fig. 4. Because of interference with the fiber, the droplet actually looks more elliptical than spherical. Thus we used a characteristic diameter D, which was defined as [7]

$$D = (D_h^2 D_v)^{\frac{1}{3}} \quad (1)$$

where D_h and D_v are the horizontal and vertical diameters of the droplet, respectively. The burning process clearly consists of several distinctive stages, which are denoted in Figs. 3 and 4 and will be discussed in the following.

3.1.1. Preheating and ignition stage (stage I)

In the preheating and ignition stage (Fig. 3a), evaporation occurred on the droplet surface, and a vapor cloud was formed surrounding the droplet. Evaporation tended to decrease the droplet size, but the droplet swelled slightly because of heat transfer from the heating wire. The overall droplet size decreased only slightly, as shown in Fig. 4. The droplet's temperature rose quickly after ignition.

The liquid component of the droplet consists of *n*-decane and 2.5 wt.% Sorbitan Oleate, which were homogeneously mixed initially. However, *n*-decane has a much lower boiling point than the surfactant (Table 1). As a result, *n*-decane, as the more-volatile component, should be vaporized first, giving the surfactant a higher concentration at the droplet surface. As *n*-decane continues to diffuse outwardly and vaporize, more and more surfactant remains near the droplet surface and eventually may form a thin layer surrounding the droplet. The diffusion behavior of multicomponent mixtures have been discussed by Law [27].

3.1.2. Classical droplet combustion stage (stage II)

The second stage is characterized by steady evaporation and burning of the droplet (Fig. 3b). This is similar to the classical burning behavior of a single-component droplet. A distinct flame envelope was formed surrounding the droplet. The luminous area atop the flame indicates soot formation. The droplet diameter decreased steadily with time, approximately following the classical D^2 law as shown in Fig. 4. During this stage, a small amount of nano-Al particles were ignited, and the burning particles rose quickly to form multiple streaks, as shown in Fig. 3c.

The temperature history of the droplet shown in Fig. 4, however, behaves differently than that of a single-component droplet; i.e., oscillations were observed around a temperature of 515 K. As we will discuss in detail in the following sections, we observed that small bubbles started to form inside the droplet later during this stage. The bubbles grew bigger and bigger and eventually merged into a single big bubble. The temperature oscillation may be due to bubble formation inside the droplet because the thermocouple tip may be exposed to the liquid at one time and to the vapor at another, resulting in oscillations. As bubbles were forming and growing later in this stage, the droplet began to oscillate and the envelope flame surrounding the droplet was distorted. This stage was ended by the disruption behavior of the droplet when the big bubble eventually ruptured.

3.1.3. Microexplosion stage (stage III)

Near the end of stage II, oscillation of the droplet became more and more intense until the first disruption took place. The droplet size was expanded by a factor of about 2 just before the disruption event because of the bubble formation and growth inside the droplet. At the moment of disruption, one smaller droplet, or at most a few, was ejected from the primary droplet. The emitted fragmented droplet(s) is typically much smaller than the primary droplet. Moreover, particles or particle aggregates were also ejected during this event. The ejected droplet(s) and particle aggregates were then ignited and burned, resulting in local flames (Fig. 3d) that caused disturbance to the envelop flame around the primary droplet. Although we call this phenomenon a microexplosion, it is slightly different from the microexplosion concept in multicomponent liquids or water/oil emulsion (fragmentation of liquid droplets resulting from violent internal gasification) because it involves fragmentation and subsequent burning of both liquid droplets and particle agglomerates. After the first microexplosion, the droplet expanded again and a second microexplosion took place. This swell-and-contract process repeated several times until most of the liquid fuel was consumed. This is also reflected by the droplet size curve during stage III in Fig. 4.

The microexplosion phenomena have been studied extensively for multicomponent liquid droplets as well as for water/oil emulsion. They are characterized by a sudden fragmentation of droplets, which may potentially enhance atomization. Law [27] explained the basic mechanism responsible for microexplosion based on the diffusion-limit model. The droplet surface becomes more concentrated with the less volatile, high-boiling-point component, and the droplet interior has a higher concentration of the more volatile, low-boiling-point component. The latter can be heated beyond its local boiling point, leading to an onset of homogenous nucleation and intense internal pressure buildup and thereby to the catastrophic fragmentation of the droplet. This theory can mostly explain the disruption phenomena we have observed for the *n*-decane/surfactant/nanoparticle mixture as a result of different physical properties between *n*-decane and surfactant. However, the addition of reactive nanoparticles complicates the process because of particle-phase dynamics and reactions, e.g., particle diffusion, aggregation, and chemical reaction, which can also affect the liquid-phase behavior. This will be elaborated on later in Section 3.3.

At the end of this stage, nearly all the liquid fuel was consumed, and the envelop flame became weaker and eventually became extinguished. A large amorphous agglomerate was left on the fiber (Fig. 3e). A magnified view of the agglomerate reveals its porous structure with exploded holes and cracks on the surface resulting from the microexplosion.

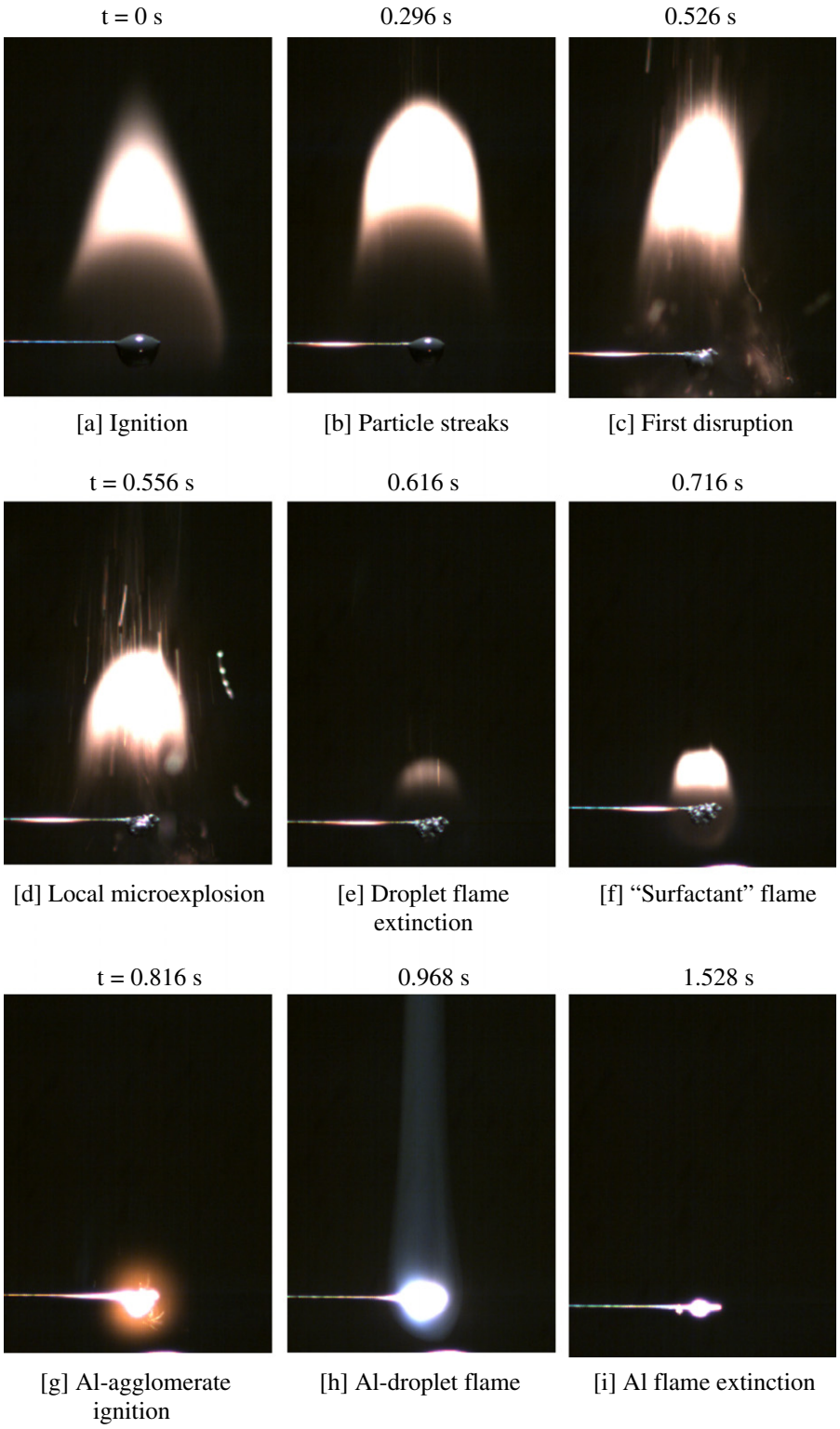

Fig. 3. A burning sequence of a stabilized *n*-decane/nano-Al droplet. The nano-Al (80 nm) concentration is 10 wt.%. The surfactant concentration is 2.5 wt.%.

3.1.4. Surfactant flame stage (stage IV)

At the end of stage III, the envelope diffusion flame went off. Shortly after that, a second flame was initiated around the large agglomerate. It lasted for a short period, about 0.1 s (Fig. 3f), before it was extinguished. The appearance of the flame is somewhat like an envelope diffusion flame. This stage is called "surfactant flame" because we believe it is due to combustion of the surfactant or its pyrolysis products. None of the previous studies of slurry fuels involving micron-sized particles [6–19] has ever reported an observation of this flame. This stage occurred for all fuel mixtures with surfactant, regardless of the type of base fluid, particle size, or particle concentration. It did not occur, however, when surfactant

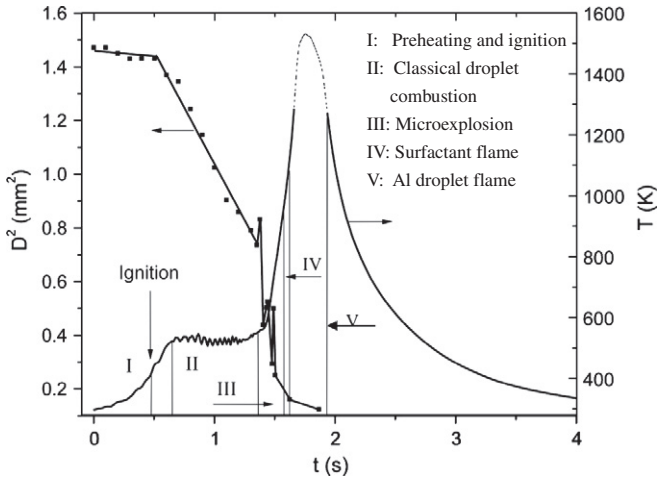

Fig. 4. The droplet size and temperature histories for a stabilized *n*-decane/nano-Al droplet.

was not added. Furthermore, when we added more surfactant to the mixture, keeping all other parameters unchanged, this flame lasted longer.

Considering that this flame is quite likely due to combustion of the surfactant or its pyrolysis product(s), we find it worthwhile to examine the chemical properties of the surfactant. Ref. [9] shows that the surfactant starts to pyrolyze at a temperature as low as 125 °C (398 K). When the temperature reaches 500 °C (773 K), the weight of the remaining liquid is less than 2%. It can be seen from Fig. 4 that the droplet temperature reaches 900 K during this stage, and thus most of the surfactant inside the particle agglomerate will be pyrolyzed. The pyrolysis product(s) inside the particle aggregate may start to diffuse out and react with oxygen when *n*-decane is almost consumed. This forms a flame that was observed in the experiment. This flame lasts only for a short period of time because typically only a small amount of surfactant was added to the fuel mixture.

3.1.5. Aluminum droplet flame stage (stage V)

The extinction of the surfactant flame was followed by ignition of the large Al agglomerate (Fig. 3g). Until then, oxygen had the chance to diffuse onto the surface of the agglomerate and caused second-phase oxidation. Shortly after it was ignited, the agglomerate was melted down and coalesced into a liquid droplet. The vapor-phase Al flame is characterized by a halo and smoke tail (Fig. 3h). The smoke tail is due to a diffusion of the aluminum oxide outwardly and upwardly. The aluminum droplet flame lasted for about 0.4 s, which is comparable to the duration of the classical combustion stage. Smaller agglomerates were occasionally ejected from the primary droplet, resulting in bright streaks.

These observations are consistent with the four steps of aluminum agglomerate combustion described by Segal and Shyy [28], which include heating aluminum particles to the melting point (around 933.1 K), ignition in the vapor phase with the local temperature exceeding the melting point of oxide (around 2320 K), two competing mechanisms during Al combustion (vapor-phase oxidation producing smoke and oxidation producing large caps), and fragmentation of particles resulting from dynamic forces in the environment. Note that the K-type thermocouple used in the experiment works only in the range of 73–1523 K. Therefore, as indicated by the dashed part of the temperature history curve, the thermocouple was unable to measure the temperature of the Al droplet, which can be as high as 2320 K (the melting point of Al oxide). Nevertheless, the steep curve in stage IV indicates a rapidly rising temperature and an intense heat release.

Lastly, a large agglomerate remained on the tip of the fiber after Al combustion was completed. Figure 5 shows a SEM image of the combustion residue, which is a porous agglomerate with a size of about 300 μm. The nonspherical shape is mainly due to interference of the Si–C fiber, which was positioned horizontally for better suspension of the droplet. Energy-dispersive X-ray spectroscopy (EDX) was conducted at several locations of the agglomerates to analyze the composition of the combustion residue. The results show that the combustion residue is primarily composed of Al and O, with a small amount of C, Mg, and Ca traces, and the measured element weight ratio of Al/O is 0.675.

3.2. Distinctive combustion stages for micron suspension

As stated earlier, the major goal of the present study is to explore the differences between nanosuspensions and micron suspensions and to understand the effects of particle size on suspension quality and the overall burning characteristics, especially particle agglomeration within a combusting droplet. Therefore we considered two micron-sized aluminum samples with a mean size of 5 and 25 μm, respectively. The procedure of preparing the microfluid-type mixtures is the same as that of preparing the nanofluid types.

For the 25 μm Al particles, the particles could not be ignited. They merely formed a large agglomerate after all liquid was consumed. The droplet-burning process is essentially the same as that for a pure liquid droplet. We know that the oxide layer around Al particles must be melted first, and ignition requires the local temperature to exceed the melting point of Al oxide so that the elemental metal can be vaporized and burned. The heat required for melting the Al oxide and the ignition temperature both increase with increasing particle size [1]. For the 25-μm particles, heat from the flame may be insufficient to melt the oxide layer; thus ignition cannot be achieved.

Figure 6 shows the burning sequence of a stabilized *n*-decane/micron-Al (5 μm) droplet. The particle concentration (10 wt.%) and the surfactant concentration (2.5 wt.%) are the same as the nanosuspension (Fig. 3) for the purpose of comparison. The histories of the droplet size and temperature are shown in Fig. 7. For this

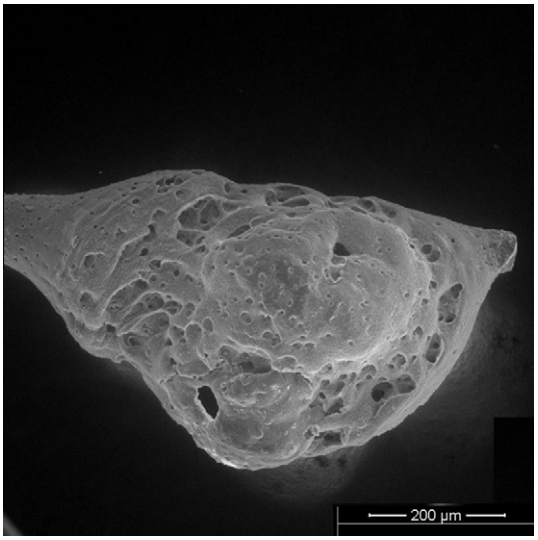

Fig. 5. SEM photograph of the combustion residue of a stabilized *n*-decane/nano-Al droplet.

example, the burning process consists of only three distinctive stages: the preheating and ignition, classical combustion, and microexplosion. Figure 8a and b show SEM photographs of the combustion residue of the *n*-decane/micron-Al droplet. It can be seen that after the microexplosion event, only a small amount of residue (Fig. 8a) was left on the Si–C fiber, and most residues (Fig. 8b) were found on the bottom and wall of the combustion chamber consisting of irregular burned agglomerates in various sizes. The residue left on the fiber consists mostly of less-agglomerated spherical particles. The EDX analysis of these particles shows that the residue primarily comprises Al, O, Si, and C with a small amount of K, Cl, and Na traces. Si and C are due to the existence of the silicon carbide fiber. The measured weight ratio of Al/O is 0.494. This ratio is lower than that for the nanoparticle case (0.675), indicating that combustion of the large nano-aluminum agglomerate is not complete.

Although there are some similarities between the two suspensions, the major differences exist in terms of burning characteristics. First of all, the amount of micron-sized particles that were ignited and burned during the classic combustion stage is much less than the amount of nanoparticles that burned during the classical combustion stage. The reason for this is because nanoparticles are lighter and diffuse faster. Thus they are easier to be brought to flame zone where the temperature is much higher than the droplet inside, reaching the boiling temperature of the oxide

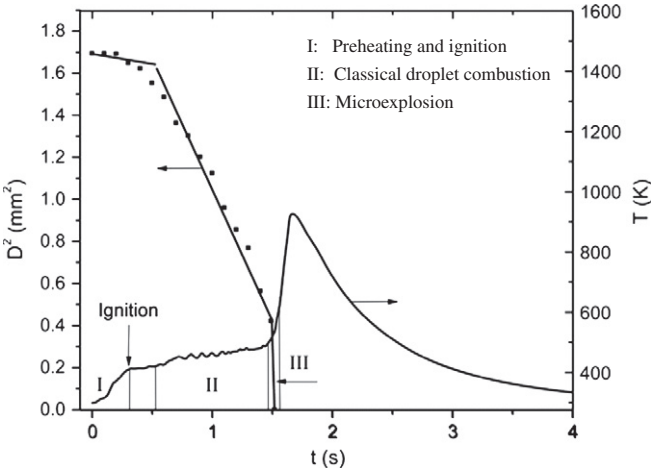

Fig. 7. The droplet size and temperature histories for a stabilized *n*-decane/micron-Al droplet.

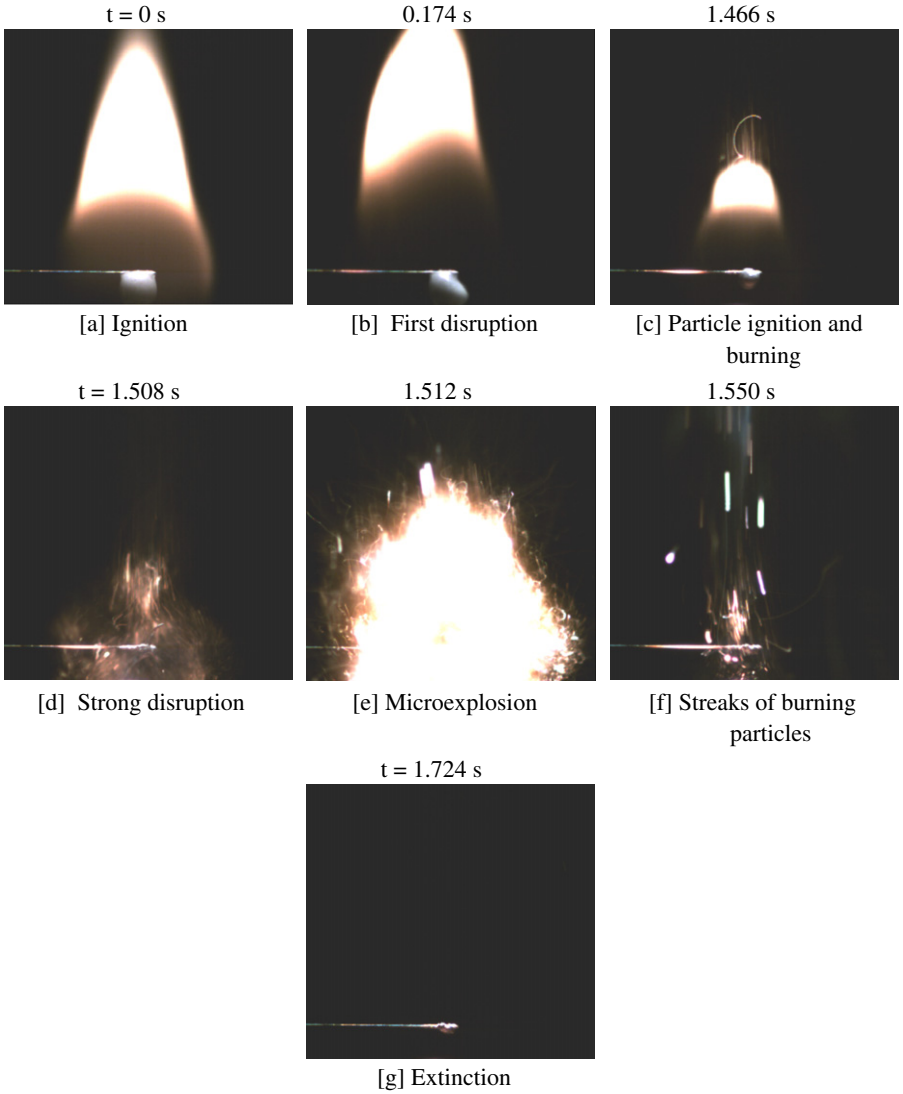

Fig. 6. A burning sequence of a stabilized *n*-decane/micron-Al droplet. The micron-Al (5 μm) concentration is 10 wt.%. The surfactant concentration is 2.5 wt.%.

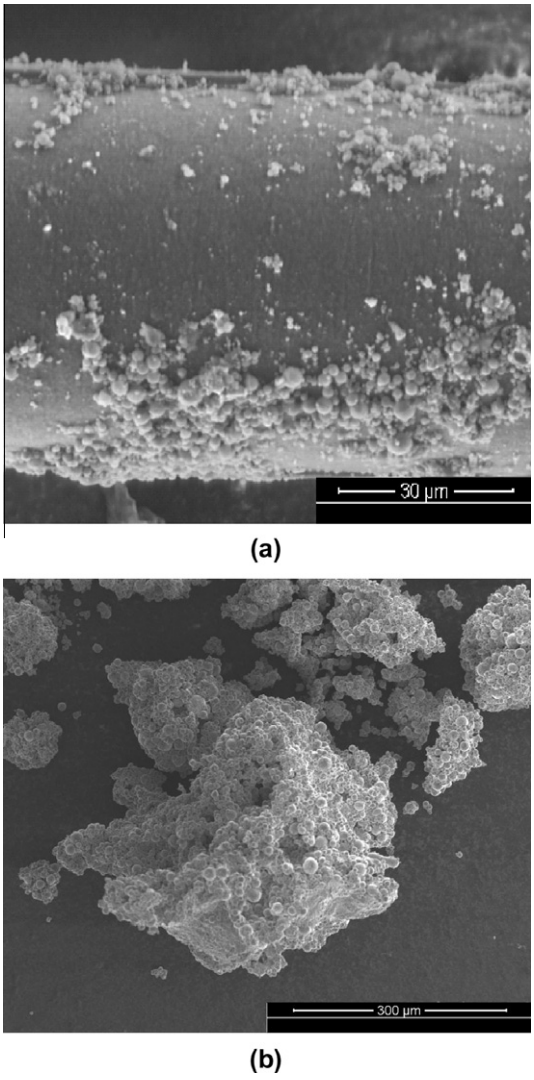

Fig. 8. SEM photographs of the combustion residue of a stabilized *n*-decane/micron-Al droplet: (a) the combustion residue left on the fiber; (b) the combustion residue collected from the chamber.

shell of particles and resulting in ignition. Second, disruption of the primary droplet as well as the microexplosion of droplet and particle agglomerate fragments are both much stronger for the micron suspension than for the nanosuspension. In fact, in the latter situation, the particle aggregate was suddenly ruptured during the microexplosion, and most of the particles were burning during this event. No obvious agglomerate was left on the fiber. Consequently, no Al droplet flame was observed, which is also reflected by the much lower peak temperature in Fig. 7.

Figure 9 compares the droplet/particle-aggregate fragmentation behavior using backlight for the two suspensions. For the micron suspension, many smaller droplets as well as fragmentation of particle aggregate were suddenly ejected from the primary droplet, causing a massive explosion. The intense disruption of the primary droplet and the explosion of particles shortened combustion time. Combustion of the large agglomerate of nanoparticles requires more time and may not be complete because of the oxide shell formed on the outer layer. This indicates that nanosuspensions may be less efficient than micron suspensions, though they have much better suspension quality. The cause for the burning difference will be discussed later in Sections 3.4 and 3.5.

3.3. Effect of the surfactant

The effect of surfactant on suspension stability, including the steric stabilization mechanism, has been discussed earlier. Surfactant also plays an important role in combustion behavior, i.e., it is responsible for the disruption behavior of the primary droplet. Without a surfactant, the burning process of a droplet containing either nanosized or micron-sized particles is characterized by only three distinctive stages: preheating and ignition, classical combustion stage and aluminum droplet flame stage. The intensity of the disruption behavior increases, and the time delay to disruption behavior decreases as the concentration of surfactant increases, which is consistent with previous studies of slurry fuels [6,8,9,16]. Furthermore, the agglomerates that formed after all liquid fuel is consumed are different with or without surfactant. With surfactant, they are porous with exploded holes and cracks on the surface because of the microexplosion. Without it, however, the surface is smooth because no microexplosion has occurred.

To better understand the role of surfactant in the overall burning process, we did experiments of *n*-decane/surfactant droplet combustion without adding any particles, and the surfactant concentration remained the same at 2.5%. The purpose was to exclude complexity caused by particles and to get a better idea of the two-component liquid mixture. The droplet size and temperature histories are shown in Fig. 10. Figure 11 shows the process of bubble formation, growth, and merging, which eventually causes droplet breakup. After ignition, relatively small bubbles were observed rising inside the droplet (Fig. 11b), and the number of bubbles and volume they occupied increased as the droplet size decreased (Fig. 11c). At a certain point, all these bubbles were observed to merge into one big bubble, as shown in Fig. 11d. The microexplosion occurred immediately after that, featured by rupture of the big bubble and ejection of smaller droplets (Fig. 11e). The swelling and microexplosion repeated several times until all the liquid fuel was consumed.

This behavior is consistent with previous studies [27] of two or multicomponent liquid mixtures. The more-volatile component, which is *n*-decane in this study, will be vaporized first when exposed to heat. The droplet surface is more concentrated with surfactant as more *n*-decane is consumed, and a thin surfactant layer will be formed around the droplet surface. Since droplet temperature is controlled by its less volatile component, the droplet core temperature could be higher than the boiling point of *n*-decane. The superheat accumulated after the droplet is heated beyond the boiling point of *n*-decane will result in the nucleation of *n*-decane, which explains the formation of bubbles inside the droplet described in the previous section. Pressure build-up inside the bubbles will ultimately break the surface tension by surfactant layer, which will result in disruption of the primary droplet.

3.4. Effect of the base fluid

As discussed earlier, suspension of nano-Al in ethanol is much longer and much better than in *n*-decane because of its higher viscosity and the tendency to form a gel structure around Al particles. Next we will discuss the effects of the base fuel on the droplet combustion characteristics of the suspensions.

Figure 12 shows the burning sequence of a stabilized ethanol/nano-Al droplet. For the purpose of comparison, formulation of the suspension is the same as the *n*-decane/nano-Al suspension shown in Fig. 3, with 10 wt.% nano-Al (80 nm) and 2.5 wt.%. surfactant. And the same procedure was adopted to prepare the mixture. The burning characteristics are similar for the two suspensions, including these stages, shown in Fig. 12: preheating and ignition, classic droplet burning, microexplosion, surfactant flame, and Al vapor flame. However, some differences exist. First of all, the

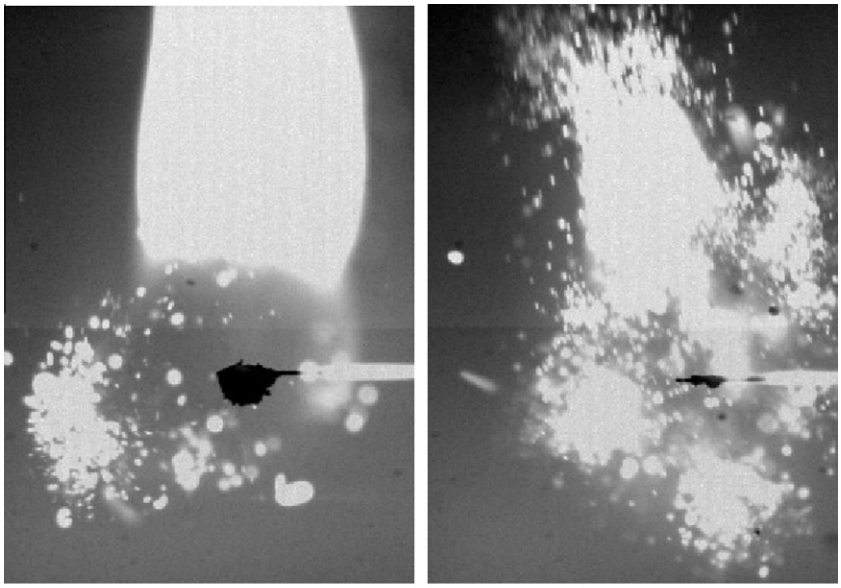

Fig. 9. Comparison of the microexplosion behavior for stabilized droplets with: (a) nanosized particles; (b) micron-sized particles.

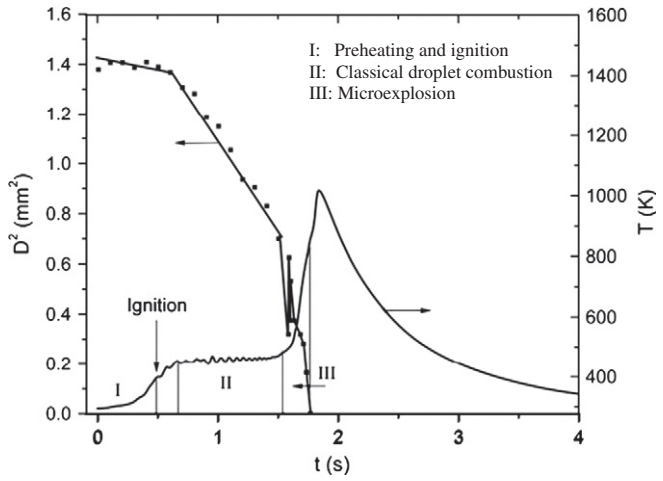

Fig. 10. The droplet size and temperature histories for an *n*-decane/surfactant droplet.

ethanol/nano-Al droplet experienced the swell-and-contract process with smaller droplets ejected from the primary droplet even before the primary droplet was ignited. This behavior can be explained by the lower boiling point of ethanol (352 K) compared to *n*-decane (447 K). Because of its high volatility, the ethanol near the droplet surface was quickly vaporized and a surfactant layer was formed around the droplet. The ethanol inside the surfactant layer was rapidly heated beyond its boiling point, even before ignition took place, and nucleation and pressure build-up inside the droplet resulted in droplet fragmentation.

Another difference is that fragmentation of the primary droplet is much more intense for the ethanol/Al droplet than for the *n*-decane/Al droplet. Moreover, the frequency is higher. This is because the difference between the boiling points of ethanol and the surfactant is larger than that between the boiling points of *n*-decane and the surfactant. As a result, more particles were burned during the classic droplet burning stage and the microexplosion stage for the ethanol/Al droplet than for the *n*-decane/Al droplet.

3.5. The droplet-drying experiment

The different microexplosion behavior between the nanosuspension and the micron suspension is quite likely caused by differences in structure and strength of particle agglomerates formed during droplet evaporation and combustion. It is necessary to review theories on microexplosion behavior that have been proposed based on previous experiments of slurry fuels involving micron-sized particles. Takahashi et al. [8] proposed a three-step mechanism based on observations of burning JP-10/boron slurry droplets, which includes the d^2-law combustion, shell formation, and disruption stages. Byun et al. [13] proposed a stage in addition to those of Takiyuki's, called the pressure buildup stage. Two mechanisms to cause pressure build-up in droplet interiors were analyzed. First, the porous shell consisting of particle layers accumulated near the surface resists the flow of liquid fuel vapor; thus a pressure increase will follow. Second, the shell temperature can exceed the boiling point of the liquid fuel, reaching the surfactant pyrolysis temperature, and the pyrolysis renders the shell texture less permeable to the fuel vapor, causing significant pressure buildup within the droplet. Wong et al. [9], however, stated that a disruption mechanism other than the one proposed by Takahashi et al. or Byun et al. may also exist, in which the formation of an impermeable shell promoted by pyrolyzed surfactant is the key event.

Although these theories have discrepancies, one common thing among them is that they all proposed that a hollow, densely packed shell was formed during the early stage. This shell may become impermeable later because of decomposition and cross-linking of the surfactant, and eventually it fragmented and caused a microexplosion as a result of inside pressure buildup. Lee and Law [10] experimentally studied the shell characteristics of JP-10/carbon slurries. They determined carbon agglomerate shell thickness, porosity values, and critical thickness at the point of shell formation. Unlike the other experiments, the carbon agglomerates in this study were not ignited at the moment of microexplosion and thereafter. Therefore the fragmented agglomerates can represent the characteristics of the shell formed in the early stage. The fragmented agglomerates were observed to be hollow with little or no internal structure and to have a thin wall (2–7 μm)

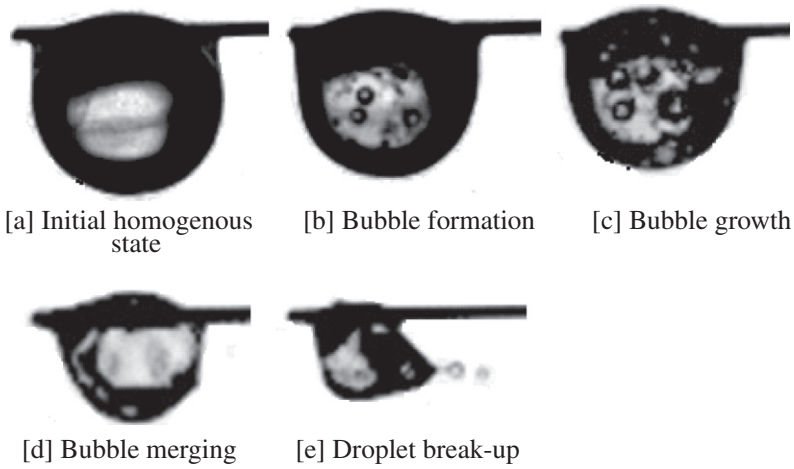

Fig. 11. A burning sequence of an *n*-decane/surfactant droplet that shows the process of bubble formation, growth, merging, and eventually droplet breakup. The surfactant concentration is 2.5 wt.%.

consisting of individually packed carbon particles roughly 0.3 μm in size. The exterior is typically smooth, except for several cracks and blowholes resulting from the fragmentation/microexplosion event.

For the nanosuspension, however, the particle agglomerate formed was believed to have a different nature than that for the micron suspension. i.e., a more-uniformly distributed spherical aggregate was observed to have formed, rather than a thin shell. To better understand the effects of particle size on shell formation and shell characteristics, we did droplet-drying experiments. Although the drying process is different from the combustion process that seems much more complicated, it can at least give us some insights on shell formation during the early stage of the droplet evaporation process. Moreover, the drying experiments may help us understand the interactions of the pyrolytic process of the surfactant and the shell/aggregate formation process of the particles by removing the base fluid. The droplet was initially suspended on the same Si–C fiber as that used in the burning experiment. It was then dried in an electric oven maintained at a constant temperature of about 400 K for about one hour until all liquid fuels were vaporized. By then, only an agglomerate was left on the tip of the fiber. The drying temperature (400 K) is below the boiling points of *n*-decane and surfactant. Under this temperature, *n*-decane could be slowly vaporized only without nucleation and ignition. For the surfactant, however, part of it will be decomposed and the rest vaporized.

Figures 13 and 14 show the SEM images of agglomerates after drying for the nanosuspension and micron suspension, respectively. An elliptical aggregate with smooth surface, which seems rigid and nonporous, was formed on the fiber by nanoparticles, shown in Fig. 13a. However, a detailed view (Fig. 13b) reveals that the surface is actually porous and that nanoparticles are bonded with one another through certain cross-linking structure. The shell formed by micron-sized particles is featured by a rather coarse surface, shown in Fig. 14a. A further magnified view (Fig. 14b) shows that the surface is nonporous, impermeable, and with micron-sized particles bridged by certain smooth structures. EDX results show that the smooth structure consists mainly of carbon. The smooth structure and the cross-linking structure bonding micron particles and nanoparticles, respectively, are believed to be the pyrolysis residue of the surfactant. Until now, we believed that carbonization of the long chain and high-weight surfactant is responsible for the bonding structure, which explains why the EDX results detect that these bonding structures consist mainly of carbon.

The results of the droplet-drying experiments further suggest that the different disruption/microexplosion behavior could be due to the characteristics of particle agglomerates: a porous aggregate that is more-uniformly distributed in a sphere for the nanosuspension vs. a densely packed, impermeable shell for the micron suspension. Furthermore, carbonization of the surfactant pyrolysis products results in an impermeable shell for the micron suspension, i.e., carbon atoms bridge aluminum particles. In regard to nanosuspension, the pressure accumulation inside the shell resulting from nucleation of *n*-decane and bubbles could be partly released through the porous structure before microexplosion. This explains why only part of the agglomerate was ejected and burned, as shown in (Fig. 9a). However, the impermeable densely packed shell formed by microparticles inhibits pressure release, and the accumulated pressure results in much stronger shell fragmentation and microexplosion (Fig. 9b).

3.6. Particle collision mechanisms and aggregation rates

The experiments have shown that the structure and strength of the aggregate formed during droplet evaporation and combustion play important roles in the overall burning characteristics of the two-phase suspension. An understanding of particle transport and aggregation mechanisms may help explain the observed difference between the nanosuspension and micron suspension. It is obvious that detailed modeling of the transient aggregation process in a burning droplet is extremely complicated and may deserve a separate study. Thus the purpose here is to understand the effect of particle size on particle collision mechanisms and aggregation rates, which will help to explain the differences in the agglomeration characteristics and subsequently the burning behavior. The analysis of particle agglomeration inside a dynamic droplet, discussed below, has not been considered by previous studies of slurry fuels.

Particle aggregation is caused by the transportation of particles, which leads to interparticle collisions, and by the attachment of colliding particles, which leads to aggregates [29]. In other words, aggregation depends on collision frequency and collision efficiency. Here, we assume that the collision efficiency is the same for particles of different sizes and for different aggregation mechanisms. Also, we assume no breakup of aggregates. In solid/liquid suspension, three major transport mechanisms are responsible for aggregation: Brownian diffusion, fluid motion, and differential setting [29]. The Brownian motion, also called perikinetic collisions, is due to random movements of small particles. Following

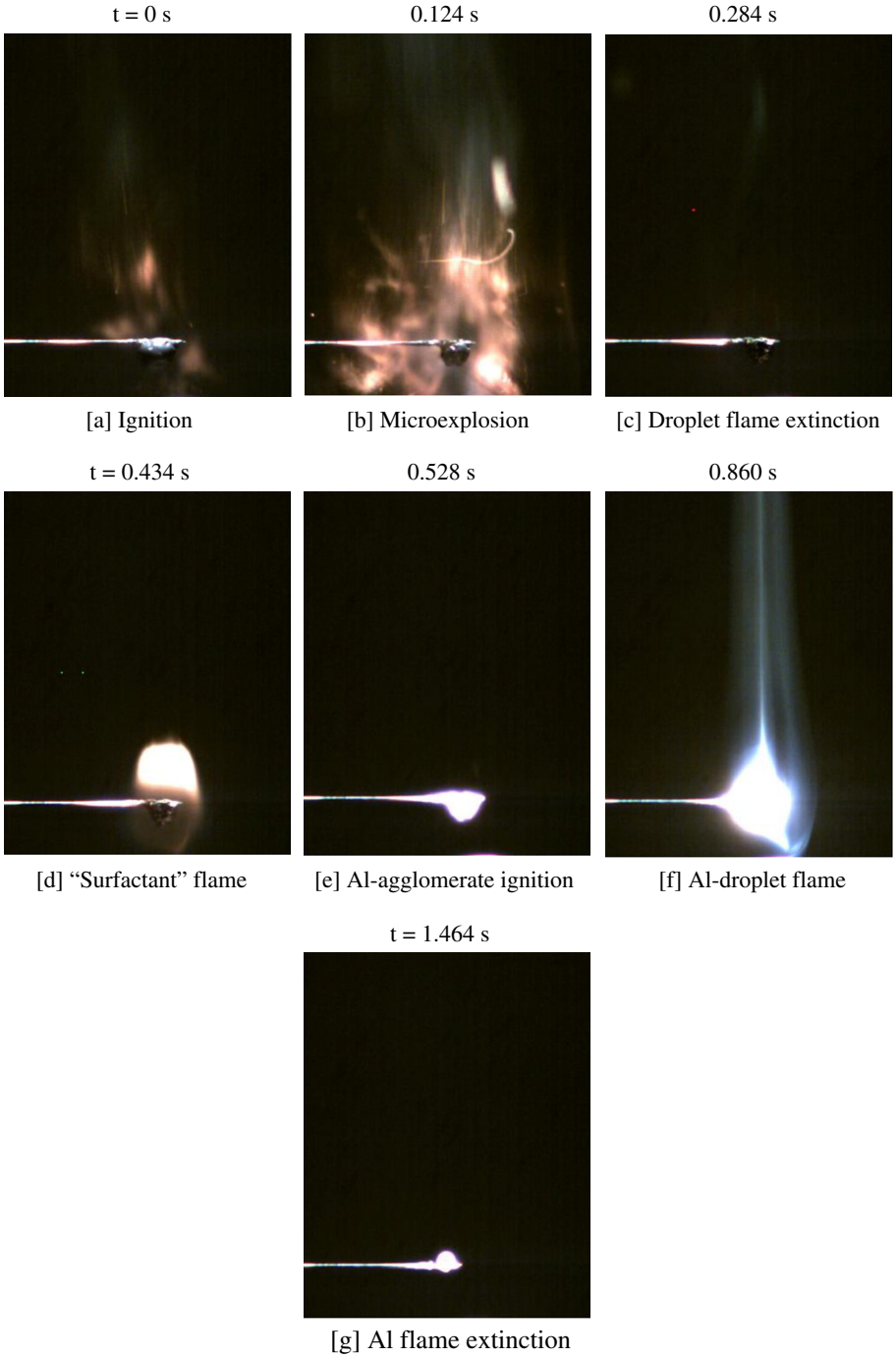

Fig. 12. A burning sequence of a stabilized ethanol/nano-Al droplet. The nano-Al (80 nm) concentration is 10 wt.%. The surfactant concentration is 2.5 wt.%.

the classic work of Smoluchowski [30], we can express the rate constant of perikinetic collisions as follows:

$$K_{i,j} = \frac{2kT}{3\mu}\frac{(r_i + r_j)^2}{r_i r_j} \tag{2}$$

where k is the Boltzmann constant, T is the temperature, μ is the viscosity of the liquid, and r_i and r_j are diameters of particles i and j, respectively. If the two colliding particles have approximately equal size, the collision rate constant $k_{i,j}$ is almost independent of particle size. This serves better for the nanosuspension at the initial stage than for the micron suspension because the nanoparticles have a more-uniform size distribution (Fig. 1a) than the micron particles (Fig. 1b). Under these conditions, the rate constant can be expressed as

$$K_{i,j} = \frac{8kT}{3\mu} \tag{3}$$

To evaluate the collision rate due to Brownian motion, we used the viscosity of n-decane (0.92 mPa s) and a temperature of 500 K to represent the temperature inside the droplet.

The second mechanism of particle transport is relative motion of particles induced by fluid motion, e.g., shear flow, stirring, and turbulence. This mechanism is also called orthokinetic aggregation [29], and it can give an enormous increase in the rate of interparticle collision, especially for large particles. In the following, we

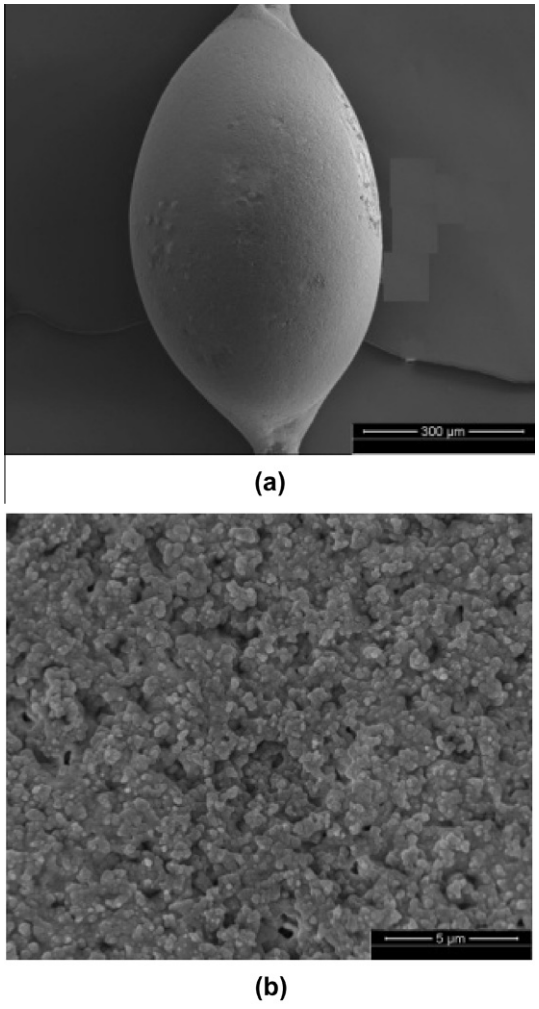

Fig. 13. SEM photographs of the dried agglomerate for a stabilized *n*-decane/nano-Al droplet: (a) overall view; (b) magnified view of the surface.

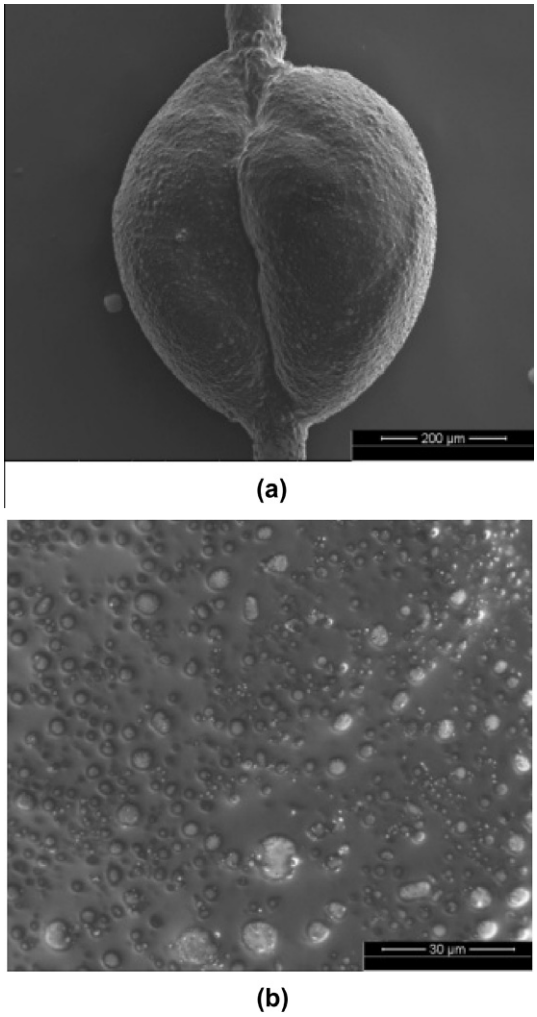

Fig. 14. SEM photographs of the dried agglomerate for a stabilized *n*-decane/micron-Al droplet: (a) overall view; (b) magnified view of the surface.

will discuss several motions of the fluid within an evaporating and burning droplet as illustrated in Fig. 15, which are also responsible for particle collisions and aggregation.

First of all, strong internal circulation was observed inside the droplet, especially during the early stage of droplet burning, which was characterized by an intense random motion of particles. Internal circulation resulting from relative velocity between droplets and surrounding gases has been studied mostly for droplets under forced convection at high Reynolds numbers and high Grashoff numbers [31], which can lead to separation and complex recirculation patterns. However, even for droplets in a stagnant environment, like those in the present experiment, natural convection can induce a relative velocity exerting a shear stress on droplet surface and thus cause internal circulation within the droplet, which has been diagnostically proved using laser-induced fluorescence [32]. Furthermore, surface tension gradients as a result of spatial variations of temperature or composition along the interface have a profound effect on droplet dynamic behavior. Raghavan et al. [33] studied internal circulation resulting from the thermal Marangoni effect (surface tension gradient because of temperature gradient) and the solutal Marangoni effect (surface tension gradient because of composition gradient). These gradients enable surface tension forces to come into play, which causes rapid and complex circulatory flow patterns within the liquid phase. The ratio of surface tension force induced velocity can be 500 times greater than the ambient velocity.

Internal circulation within a droplet can be very complicated. To simplify the problem, we propose a simple model (Fig. 16) to represent the internal circulation motion. In this model, the fluid rotates circularly at a constant speed, and the velocity varies linearly in the direction of the radius. Particles will follow the circular streamlines and collide with particles moving on different streamlines because of their relative motions. Following the classic analysis of Smoluchowski for uniform laminar shear flows [30], we consider two particles, i and j, with a radius of r_i and r_j, respectively. Considering a fixed central sphere of radius r_j and flowing particles of radius r_i, we can assume that those moving particles on streamlines that bring their centers within a distance $r_i + r_j$ of the central particle will collide with it. The collision frequency can then be derived by considering the flux of particles through a curved cylinder of radius $r_i + r_j$, the axis of which passes through the center of the fixed sphere j. By calculating the swept-volume of a circular area of radius R_{ij}, we find that the total number of collisions occurring between i and j particles in unit volume and unit time is given by

$$J_{ij} = 2n_i n_j \int_0^{R_{ij}} 2Gr\sqrt{R_{ij}^2 - r^2}\,dr = \frac{4}{3} n_i n_j G(r_i + r_j)^3 \tag{4}$$

where G is the velocity gradient or shear rate, n_i and n_j are particle number densities.

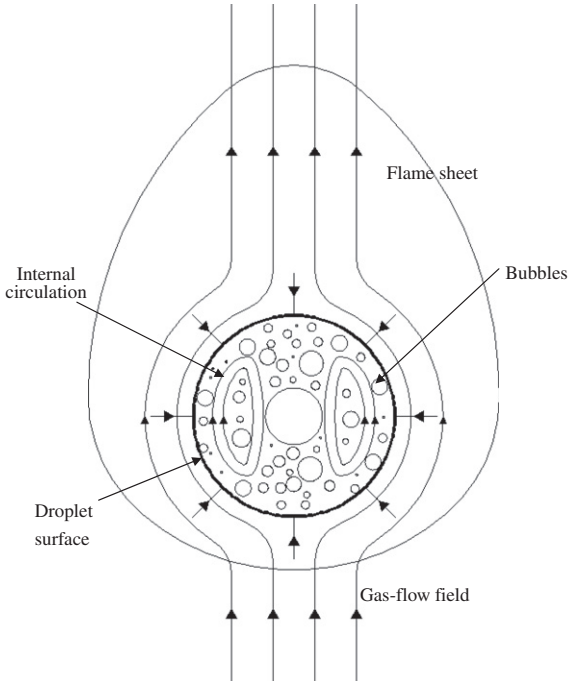

Fig. 15. Illustration of the flow pattern and motions around and within a burning three-component (*n*-decane + surfactant + Al-particles) droplet.

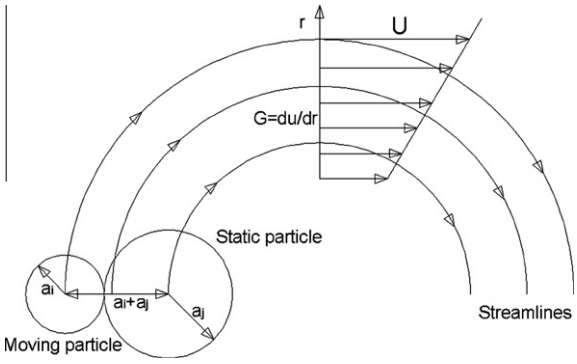

Fig. 16. A simple model for estimation of the orthokinetic collision rate resulting from internal circulation within the droplet.

To estimate particle collision rate in a droplet because of internal circulation based on Eq. (4), we used a velocity distribution based on the numerical simulations of Yang et al. [34], which were for an isothermal sphere droplet under natural convection condition. The internal circulation velocity near the droplet surface, which is of the same order as the maximum gas velocity around the droplet, is about 2 cm/s. Therefore the value of G is around 40 s^{-1}. The particle collision rate resulting from internal circulation then can be estimated using Eq. (4).

Besides the internal circulation, the fluid also moves in the radial direction. As the droplet evaporates, its surface regresses continuously, indicating that the droplet interior is experiencing a net convective velocity as the liquid element "flows" toward the surface. Because of the regressing droplet surface, the particles near the surface must move inwardly because of surface tension forces, resulting in a greater chance of colliding with the particles inside the droplet. Furthermore, the particle concentration near the droplet surface increases because of particle accumulation in that area, resulting in an increased aggregation rate. Based on the history of droplet diameter (Fig. 10), we estimate that the surface regression rate is about 0.77 mm/s for the *n*-decane droplet at the early stage. Moreover, the fluid at the center of the droplet has an outwardly diffusion velocity, which may also enhance particle collision. This velocity, however, is typically low, about two orders lower than the surface regression rate [27], and thus will not be considered.

To estimate the particle collision rate resulting from droplet surface regression, we propose a simple model in which the droplet surface has a constant regression velocity U while the inside is quiescent, as shown in Fig. 17. We consider a fixed central sphere of radius r_j of particle j and flowing particles i of radius r_i. Similar to Smoluchowski's approach, we calculate the flux of particles through a cylinder of radius R_{ij} (the collision radius, $R_{ij} = r_i + r_j$), and the axis of the cylinder passes through the center of the fixed sphere j. We can see that all particles in the cylinder will collide with the inside particle j with a constant velocity U. The total number of collisions J_{ij} occurring between any particle i and particle j can be expressed as

$$J_{ij} = n_i n_j U \pi (r_i + r_j)^2 \tag{5}$$

It is absolutely important to understand that this model applies only to the droplet surface area. Eq. (5) represents the collision rate of particles near the surface. It does not, however, represent the collision rate of particles inside the droplet, which are in fact not affected by droplet surface regression.

Lastly, bubbles were observed inside the droplet when a surfactant was added to the mixture. During the classical combustion stage, bubbles were observed to form, grow, and eventually emerge into a large bubble inside the droplet. This caused the liquid to expand and then contract, and this motion was repeated a few times. Because of bubble formation and growth, the liquid near the center was pushed outwardly, which consequently brought the nearby particles outwardly also, and the particle collision rate can be increased because of the velocity differences between particles. As the large bubble ruptured, the liquid contracted toward the center. Therefore the particles may be able to diffuse back to the center as a result of Brownian motion. However, if they have been attached to a large aggregate in previous collisions, they are less likely to diffuse back to the center.

So far, the major fluid motions (internal circulation and radial motion) that cause particle collision and aggregation have been discussed, and the collision rates of particles resulting from these motions have been estimated. We will next discuss the third mechanism of particle transport in a droplet. When particles of different size and density are settling from a suspension, they can capture other particles as they fall. It is obvious that differential settling will be more important when the particles are large, dense, and much heavier than the fluid. The appropriate rate can be calculated based on [29]

$$J_{ij} = \left(\frac{2\pi g}{9\mu}\right)(\rho_s - \rho) n_i n_j (r_i + r_j)^3 (r_i - r_j) \tag{6}$$

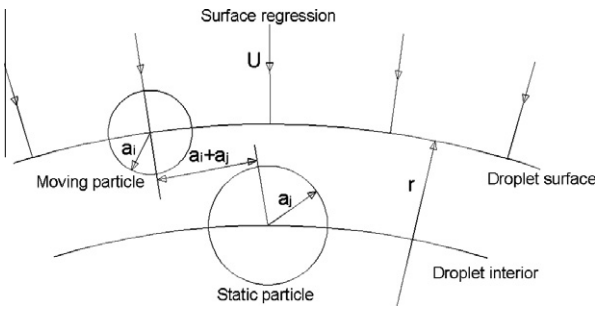

Fig. 17. A simple model for estimation of the orthokinetic collision rate resulting from droplet surface regression.

where g is the acceleration as a result of gravity, ρ_s is the density of the particles, and ρ is the density of the fluid. There it is often in the later stages of flocculation that floc growth by sedimentation becomes significant [29].

Based on the above theories and assumptions, we calculate the collision rate between a particle with a fixed size and other particles of various sizes because of various collision mechanisms. The calculated collision rate constants for nanoparticles are shown in Fig. 18, for which a particle with a fixed size of 80 nm and other particles with sizes varying from 1 to 1000 nm were considered. The rate constants were plotted as a function of particle size because of Brownian motion, internal circulation, droplet surface regression, and sedimentation, respectively. Similarly, the collision rate constants for micron particles with a fixed size of 5 μm and other particles with sizes varying from 0.05 to 5 μm are plotted as a function of particle size in Fig. 19.

The comparison between Figs. 18 and 19 clearly shows that perikinetic aggregation resulting from random Brownian motion dominates for nanoparticles, whereas orthokinetic aggregation dominates for micron-sized particles. For the micron suspension (Fig. 19), orthokinetic aggregation because of droplet surface regression and internal circulation dominates particle transport and collision, and the Brownian motion is the least important. This explains why a thin shell forms as a result of the droplet surface regressing into the droplet interior. Later on, the shell can become impermeable because of decomposition and cross-linking of the surfactant. For the nanosuspension (Fig. 18), however, perikinetic aggregation because of Brownian motion and orthokinetic aggregation because of surface regression are of the same order. However, aggregation resulting from internal circulation and differential settling is much smaller. Note that the estimated aggregation rate resulting from surface regression (Eq. (5)) can be employed only to the surface area and does not affect the internal areas. Therefore the overall effect is that perikinetic aggregation dominates within the droplet, though the density of the aggregate may be higher at the surface than at the interior. In other words, because of the random Brownian motion of nanoparticles, the particle aggregate is more-uniformly distributed and spherical, rather than being a thin shell, as for the micron suspension.

In summary, the collision rate analysis here can help explain the different burning behavior between nanosuspensions and micron suspensions observed in the experiments. For micron suspensions, the particles near the droplet surface tend to form a densely packed shell because of surface regression, and the particles inside the droplet tend to be pushed outwardly because of bubble formation, which increases the collision rate between the internal particles and the shell. The shell later becomes impermeable as a result of carbonization of the surfactant; eventually the shell suddenly fragments because of internal pressure buildup, which introduces a way of rapid and more-efficient burning of aluminum particles. For nanosuspensions, however, the random Brownian motion dominates. A porous homogenous aggregate, rather than a shell, is formed because of the fast diffusion of particles. The carbonization of the surfactant is unable to form an impermeable surface because of the surfactant's small volume and the aggregate's large volume/surface. Therefore the pressure build-up inside the droplet can be released from the porous structure, resulting in much less intense or even no microexplosion. Obviously, the analysis here is suitable for the early stage of droplet combustion, which is the time that particle aggregation starts to form. The collision rate analysis, however, cannot be approximated for the later stage when large agglomerates have already formed.

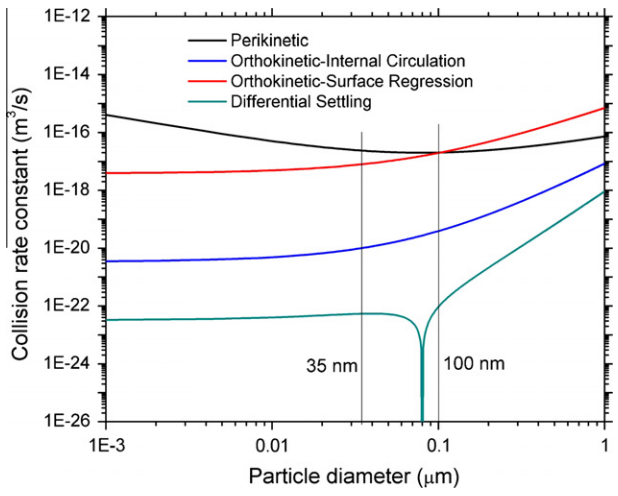

Fig. 18. Particle collision rate constants resulting from Brownian motion, fluid motion including droplet surface regression and internal circulation, and differential settling for an *n*-decane/nano-Al droplet.

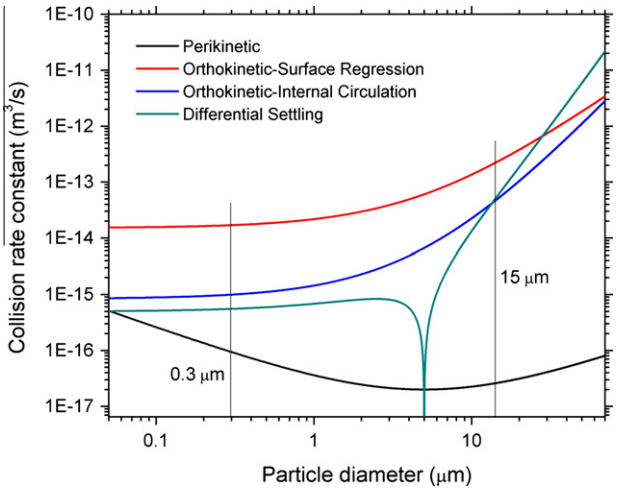

Fig. 19. Particle collision rate constants resulting from Brownian motion, fluid motion including droplet surface regression and internal circulation, and differential settling for an *n*-decane/micron-Al droplet.

4. Conclusions

The burning characteristics of *n*-decane and ethanol droplets containing nano and micron-sized aluminum particles were investigated. The emphasis was to explore the difference between nanosuspensions and micron suspensions and to understand the effect of particle size on suspension quality and droplet burning characteristics. Other factors – such as the effect of particle concentration, the type of metal particles with or without surface functionalization, and the type of the surfactants/dispersants – will be explored in future studies. In general, nanosuspensions can remain stable for a much longer time than micron suspensions, mainly because nanoparticles have higher surface-to-volume ratio; thus the interaction between particle surface and the surrounding liquid is strong enough to overcome differences in density.

Five distinctive stages (preheating, classical combustion, microexplosion, surfactant flame, and aluminum droplet flame) were identified for a stabilized *n*-decane/nano-Al droplet, while only three distinctive stages (preheating, classical combustion, and microexplosion) were identified for a stabilized *n*-decane/micron-Al with the same mass-based particle concentration and surfactant concentration. For the same solid loading rate and the same surfactant concentration, the microexplosion behavior of the

micron suspension occurred later than the nanosuspension with much stronger intensity, accompanied by intense fragmentation of the primary droplet and particle aggregate, causing a massive explosion of particles. On the contrary, nanoparticles are easier to agglomerate. Combustion of the large agglomerate requires longer time and is less complete because of the formation of oxide shell on surface.

The different burning behaviors of the micron suspension and the nanosuspension are mainly due to the different structure of particle agglomerates formed during droplet evaporation and combustion, with the former forming a densely packed, impermeable shell and the latter a porous, more-uniformly distributed spherical aggregate. A theoretical analysis shows that for nanoparticles, particle collision and aggregation are dominated by the random Brownian motion. For micron-sized particles, however, particle collision and aggregation are dominated by fluid motion (droplet surface regression, droplet expansion because of bubble formation, and internal circulation), whereas the Brownian motion is the least important. This explains the different aggregation structure we have observed for nanosuspensions and micron suspensions.

Comparisons were also made for suspensions with different base fluids, *n*-decane vs. ethanol. The results show that a stable ethanol/nano-Al suspension lasts much longer than *n*-decane/nano-Al suspension because of ethanol's tendency to form a gel structure surrounding the particles and its higher viscosity. The better suspension quality may indicate that ethanol is a good candidate for mixing with energetic nanoparticles, especially when we consider that ethanol has lower energy density than the other liquid fuels. In terms of combustion characteristics, the chief difference between the two suspensions is that microexplosion occurred even before the droplet was ignited for the ethanol/nano-Al suspension, resulting from ethanol's high volatility. Moreover, the fragmentation of the primary droplet occurred more frequently and with higher intensity because of the larger difference between the boiling points of ethanol and the surfactant. Due to this reason, more aluminum particles were burned more completely during the classical combustion stage and the microexplosion stage.

Acknowledgment

This work has been supported by the Army Research Office under contract W911NF-10-0133 with Dr. Ralph Anthenien as technical monitor.

References

[1] R.A. Yetter, G.A. Risha, S.F. Son, Proc. Combust. Inst. 32 (2009) 1819–1838.
[2] E.L. Dreizin, Prog. Energy Combust. Sci. 35 (2009) 141–167.
[3] J.J. Granier, M.L. Pantoya, Combust. Flame 138 (2004) 373–383..
[4] H. Tyagi et al., Nano Lett. 8 (2008) 1410–1416.
[5] E. Beloni, V.K. Hoffmann, E.L. Dreizin, J. Propul, Power 24 (2008) 1403–1411.
[6] P.R. Choudhury, Prog. Energy Combust. Sci. 18 (1992) 409–427.
[7] P. Antaki, F.A. Williams, Combust. Flame 67 (1987) 1–8.
[8] F. Takahashi, I.J. Heilweil, F.L. Dryer, Combust. Sci. Technol. 65 (1989) 151–165.
[9] S.C. Wong, A.C. Lin, H.Y. Chi, Proc. Combust. Inst. 23 (1990) 1391–1397.
[10] A. Lee, C.K. Law, Combust. Flame 85 (1991) 77–93.
[11] S.R. Turns, S.C. Wong, E. Ryba, Combust. Sci. Technol. 54 (1987) 299–318.
[12] S.C. Wong, S.R. Turns, Combust. Sci. Technol. 52 (1987) 221–242.
[13] D.Y. Byun, S.W. Baek, J.H. Cho, Int. J. Heat Mass Transfer 42 (1999) 4475–4486.
[14] G.A. Szekely, G.M. Faeth, Aiaa J. 20 (1982) 422–429.
[15] T. Sakai, M. Saito, Combust. Flame 51 (1983) 141–154.
[16] S.C. Wong, S.R. Turns, Combust. Sci. Technol. 66 (1989) 75–92.
[17] S.C. Wong, A.C. Lin, Combust. Flame 89 (1992) 64–76.
[18] S.Y. Cho, F. Takahashi, F.L. Dryer, Combust. Sci. Technol. 67 (1989) 37–57.
[19] P.R. Choudhury, M. Gerstein, Acta Astronaut. 25 (1991) 739–746.
[20] D.H. Napper, Polymeric Stabilization of Colloidal Dispersions, Academic, London, 1983.
[21] S.U.S. Choi, J. Heat Transfer – Trans. ASME 131 (2009).
[22] A. Gedanken, Ultrason. Sonochem. 11 (2004) 47–55.
[23] J.A. Eastman et al., Annu. Rev. Mater. Res. 34 (2004) 219–246.
[24] Y.-J. Shin, Y.-H. Shen, Chemosphere 68 (2007) 389–393.
[25] T. Kadota, H. Yamasaki, Prog. Energy Combust. Sci. 28 (2002) 385–404.
[26] D.H. Napper, J. Colloid Interface Sci. 58 (1977) 390–407.
[27] C.K. Law, Prog. Energy Combust. Sci. 8 (1982) 171–201.
[28] C. Segal, W. Shyy, J. Energy Resour. Technol. 118 (1996) 180–186.
[29] J.H. Fendler, I. Dekany, Nanoparticles in Solids and Solutions, Kluwer Academic Publishers, Boston, 1996.
[30] M. Smoluchowski, Z. Phys. Chem. 92 (1917) 129–168.
[31] W.A. Sirignano, Prog. Energy Combust. Sci. 9 (1983) 291–322.
[32] M. Winter, L.A. Melton, Appl. Opt. 29 (1990) 4574–4577.
[33] V. Raghavan et al., Combust. Flame 145 (2006) 791–807.
[34] S. Yang, V. Raghavan, G. Gogos, Int. J. Heat Fluid Flow 28 (2007) 821–837.